Real-Time Identification of Optimal Operating Points in Photovoltaic Power Systems

Weidong Xiao, *Student Member, IEEE*, Magnus G. J. Lind, *Student Member, IEEE*, William G. Dunford, *Senior Member, IEEE*, and Antoine Capel

***Abstract*—Photovoltaic power systems are usually integrated with some specific control algorithms to deliver the maximum possible power. Several maximum power point tracking (MPPT) methods that force the operating point to oscillate have been presented in the past few decades. In the MPPT system, the ideal operation is to determine the maximum power point (MPP) of the photovoltaic (PV) array directly rather than to track it by using the active operation of trial and error, which causes undesirable oscillation around the MPP. Since the output features of a PV cell vary with environment changes in irradiance and temperature from time to time, real-time operation is required to trace the variations of local MPPs in PV power systems. The method of real-time estimation proposed in this paper uses polynomials to demonstrate the power–voltage relationship of PV panels and implements the recursive least-squares method and Newton–Raphson method to identify the voltage of the optimal operating point. The effectiveness of the proposed methods is successfully demonstrated by computer simulations and experimental evaluations of two major types of PV panels, namely: 1) crystalline silicon and 2) copper–indium–diselenide thin film.**

***Index Terms*—Curve fitting, least-squares method (LS), Newton–Raphson method (NRM), parameter estimation, photovoltaic (PV) power systems, polynomials, real-time systems.**

I. Introduction

In PHOTOVOLTAIC (PV) power systems, maximum power point tracking (MPPT) is essential because it takes full advantage of the available solar energy. Two popular tracking methods based on power measurement are widely adopted in PV power systems: the perturbation and observation method (P&O) [1] and the incremental conductance method (IncCond) [2]. Actually, both P&O and IncCond are based on the same technology by regulating the voltage of the PV array to follow an optimal setpoint, which represents the voltage of optimal operating point V_{OOP}, as shown in Fig. 1. In some of the literature, V_{OOP} is also symbolized by V_{MPOP}, which stands for the voltage of the maximum power operating point.

The local maximum power operating point is continuously tracked and updated by the MPP tracker to satisfy $dP/dV = 0$, where P represents the output power of the PV array and V represents the PV voltage. By investigating the power–voltage relationship, which is the $P-V$ curve of a typical PV module, the MPPs can always be tracked if we keep dP/dV equal to zero for any solar insolation or temperature since all local MPPs have the same mathematical attribute.

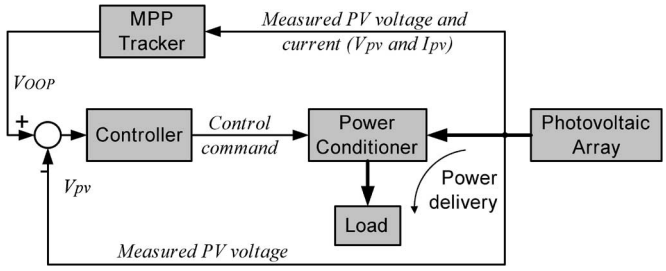

Fig. 1. Block diagram of the P&O and IncCond MPPT topologies.

The continuous oscillation around the optimal operating point is an intrinsic problem of the active P&O tracking algorithm. This causes power loss and system instability [2]. The IncCond is developed to eliminate the oscillations around the MPP. However, experiments [2] show that there were still oscillations under stable environmental conditions because the digitized maximum power condition of $dI/dV = -I/V$, which is equivalent to $dP/dV = 0$, only rarely occurred. Another drawback for both algorithms is that the perturbation step of the PV voltage setpoint is difficult to choose when dealing with the tradeoff between steady-state performance and fast dynamic response. Therefore, it is desirable to determine the V_{OOP} directly during the real-time operation, instead of tracking it simply through trial and error.

A general real-time identification method of MPP is proposed in this paper. In Section II, the modeling techniques of the PV cells used in this paper are proposed, the process of parameterization is presented, and the modeling accuracy is examined. Section III presents the principle and procedure of real-time estimation in detail based on the recommended PV model. In Section IV, the effectiveness of the proposed method is demonstrated by both computer simulation and experimental evaluation. Section V concludes the paper.

II. Modeling Techniques

One of the fundamental issues of real-time identification is the selection of model structure. It is necessary to have a mathematical model that can accurately represent the electric characteristics of the PV array and can be easily solved by analytical methods. Since the identification of the PV model is performed automatically during system operation, it is important to have a good understanding of all aspects of different models before the real-time application is implemented.

Manuscript received January 12, 2004; revised April 11, 2005. Abstract published on the Internet May 18, 2006.

W. Xiao, W. G. Dunford, and A. Capel are with the University of British Columbia, Vancouver, BC V6T 1Z4, Canada (e-mail: weidongx@ece.ubc.ca).

M. G. J. Lind is with the PACCAR Technical Center Inc., Mount Vernon, WA 98273-9690 USA.

Digital Object Identifier 10.1109/TIE.2006.878355

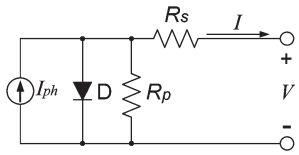

Fig. 2. Equivalent circuit of a single-diode model.

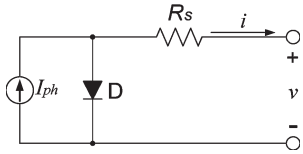

Fig. 3. Equivalent circuit of SSDM.

The traditional equivalent circuit of a solar cell is represented by a current source in parallel with one or two diodes. A single-diode model from [3], which includes four components, namely: 1) a photocurrent source $i_{\rm ph}$; 2) a diode parallel to the source; 3) a series resistor R_s; and 4) a shunt resistor R_p, is illustrated in Fig. 2. There are five unknown parameters in a single-diode model. The mathematical description of the current versus voltage characteristics for the equivalent circuit is represented by a coupled nonlinear equation, which is generally difficult to solve using analytical methods in real-time operation.

Hence, it is essential to find a simple model that would be useful for the real-time application. In the following sections, three simplified models are analyzed, and their effectiveness is examined. Without further description, the discussed modeling methods of equivalent circuits are based on the PV cells. The manufacturers usually supply solar cells in modules that consist of a number of identical solar cells connected in series. The current–voltage ($I-V$) characteristics of the series-connected cells can be simply obtained by adding the voltages of the individual cells.

A. Simplified Single-Diode Model (SSDM) of Solar Cells

It was proposed in [4] that SSDM is sufficient for representing three different types of PV cells when the temperature effect on parameterization is taken into account. The shunt resistor is removed from the model, as shown in Fig. 3. The current through a PV cell is given by

$$i = i_{\rm ph} - i_{\rm sat}\left[e^{\left(\frac{v+iR_s}{v_t}\right)} - 1\right] \tag{1}$$

$$v_t(T) = \frac{AkT}{q} \tag{2}$$

where $i_{\rm ph}$ represents the photocurrent, v is the voltage across the cell, v_t is the thermal voltage, R_s is the series resistor, and $i_{\rm sat}$ is the saturation current of the diode. The thermal voltage v_t is a function of temperature T, where A represents the ideality factor of the diode, k is the Boltzmann's constant, and q stands for the charge of an electron.

B. Further SSDM (FSSDM) of Solar Cells

The series resistor of SSDM is neglected to form FSSDM developed in [5], as shown in Fig. 4. The significance of this model is that it decouples the current–voltage relationship as

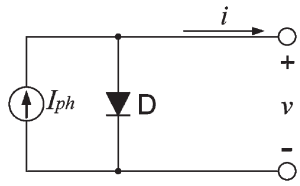

Fig. 4. Equivalent circuit of FSSDM.

$$i = i_{\rm ph} - i_D = i_{\rm ph} - i_{\rm sat}\left[e^{\left(\frac{v}{v_t}\right)} - 1\right]. \tag{3}$$

C. Polynomial Curve Fitting (PCF)

Aside from the equivalent-circuit modeling methods, the PCF is proposed in this study to represent the electric characteristics of PV modules. It was determined that a fourth-order polynomial can successfully demonstrate the output feature, which is the $I-V$ or $P-V$ curve, of PV cells made of copper–indium–diselenide (CIS) thin film. The cells made of crystalline silicon generally have higher fill factor than those of the CIS thin film. Fill factor is a measure of the squareness of the $I-V$ curve. Therefore, at least a sixth-order polynomial is required to accurately represent the characteristics of silicon cells. The unknown parameters of a polynomial model are determined by the least-squares method (LS) when the measured data of the PV voltage and current are available. To illustrate the parameterization process, a sixth-order $I-V$ relationship of a silicon cell is defined as

$$i(k) = b_0 + b_1 v(k) + b_2 v^2(k) + b_3 v^3(k) + b_4 v^4(k) + b_5 v^5(k) + b_6 v^6(k). \tag{4}$$

Variables $i(k)$ and $v(k)$ are the PV output current and voltage in the discrete time domain, respectively. The b_is are the parameters of the polynomial. For convenience of representation, the following notations of vectors and matrix are introduced:

$$Y = \begin{bmatrix} i(1) \\ i(2) \\ i(3) \\ \vdots \\ i(k) \end{bmatrix}$$

$$X = \begin{bmatrix} 1 & 1 & 1 & \cdots & 1 \\ v(1) & v(2) & v(3) & \cdots & v(k) \\ v^2(1) & v^2(2) & v^2(3) & \cdots & v^2(k) \\ \vdots & \vdots & \vdots & \ddots & \vdots \\ v^6(1) & v^6(2) & v^6(3) & \cdots & v^6(k) \end{bmatrix}$$

$$\theta = \begin{bmatrix} b_0 \\ b_1 \\ b_2 \\ \vdots \\ b_6 \end{bmatrix}. \tag{5}$$

Then, the measured output vector Y can be represented by a simple regression model, i.e.,

$$Y = X^T\theta \tag{6}$$

where X is the vector of the regression variables observed from measurements. A measure of deviation, the root mean square of the Euclidean norm of the residual vector is

$$\frac{\|\varepsilon\|_2}{\sqrt{m}} = \frac{\|Y - X^T\theta\|_2}{\sqrt{m}} \tag{7}$$

where m is the number of samples. According to the theorem of least squares curve fitting, the vector of the estimated parameters $(\hat{\theta})$ is given by [6]

$$\hat{\theta} = (X^TX)^{-1}X^TY. \tag{8}$$

D. Parameterization of the Equivalent Circuits of PV Cells

There are four parameters in SSDM and three parameters in FSSDM that need to be derived from the data obtained from experimental tests of the PV cells under three conditions, namely: 1) short circuit; 2) open circuit; and 3) MPP. According to the short-circuit situation in the equivalent circuit, the photocurrent $i_{\rm ph}$ is approximated as

$$\hat{i}_{\rm ph} \approx \tilde{I}_{\rm sc} \tag{9}$$

where $\hat{i}_{\rm ph}$ is the estimated photocurrent $i_{\rm ph}$ and $\tilde{I}_{\rm sc}$ is the measured short-circuit current at a certain test condition with constant irradiance and temperature. The photocurrent is a function of insolation and temperature.

Based on the open-circuit condition in the equivalent circuit, the saturation current $i_{\rm sat}$ of the diode is expressed as

$$\hat{i}_{\rm sat} = \frac{\hat{i}_{\rm ph}}{e^{\left(\frac{\tilde{V}_{\rm oc}}{v_t}\right)} - 1}. \tag{10}$$

The variable $\hat{i}_{\rm sat}$ represents the estimated saturation current $i_{\rm sat}$, and $\tilde{V}_{\rm oc}$ is the measured open-circuit voltage at the same test condition as that of the short-circuit measurement. The thermal voltage v_t is a function of temperature T, which needs to be determined.

The MPP $(v_{\rm mpp}, i_{\rm mpp})$ is measured through experimental tests under the identical testing environment. At the MPP of SSDM, the relationship is described as

$$i_{\rm mpp} = i_{\rm ph} - i_{\rm sat}\left[e^{\frac{v_{\rm mpp}+i_{\rm mpp}R_s}{v_t}} - 1\right]. \tag{11}$$

Substituting (9) and (10) into (11) gives

$$i_{\rm mpp} = \tilde{I}_{\rm sc} - \left[\frac{e^{\left(\frac{v_{\rm mpp}+i_{\rm mpp}R_s}{v_t}\right)} - 1}{e^{\left(\frac{\tilde{V}_{\rm oc}}{v_t}\right)} - 1}\right]\tilde{I}_{\rm sc}. \tag{12}$$

TABLE I
SPECIFICATIONS OF PV PANELS USED IN THE EVALUATION

Modules	Make	Material	Configuration	Data at STC*
Solarex MSX-83	BP solar	Cystalline silicon	36 cells in series	*Pmax = 83W* *V_{OOP} = 17.1V* *Voc = 21.2V*
Shell ST10	Shell solar	CIS thin film	42 cells in series	*Pmax = 10W* *V_{OOP} = 15.6V* *Voc = 22.9V*

*STC represents the Standard Test Condition, where the irradiance is 1000W/m^2 and the temperature is 25°C

Reorganizing (12), we obtain the relationship of R_s and v_t in SSDM

$$R_s = \frac{v_t \ln\left[\left(1 - \frac{i_{\rm mpp}}{\tilde{I}_{\rm sc}}\right)e^{\left(\frac{\tilde{V}_{\rm oc}}{v_t}\right)} + \frac{i_{\rm mpp}}{\tilde{I}_{\rm sc}}\right] - v_{\rm mpp}}{i_{\rm mpp}}. \tag{13}$$

According to the power–voltage characteristics of the PV cell, the MPPs occur when $dP/dV = 0$, where P is the PV module's output power and V is the PV voltage. The equation can be represented by

$$\left.\frac{di}{dv}\right|_{v=v_{\rm mpp}} + \frac{i_{\rm mpp}}{v_{\rm mpp}} = 0. \tag{14}$$

From (1), we have

$$\frac{di}{dv} = -i_{\rm sat}\left\{e^{\frac{v+iR_s}{v_t}}\left[\frac{1}{v_t} + \left(\frac{R_s}{v_t}\right)\frac{di}{dv}\right]\right\} \tag{15}$$

which gives

$$\left.\frac{di}{dv}\right|_{v=v_{\rm mpp}} = -\frac{\frac{\hat{i}_{\rm sat}}{v_t}e^{\left(\frac{v_{\rm mpp}+i_{\rm mpp}R_s}{v_t}\right)}}{1 + \frac{\hat{i}_{\rm sat}R_s}{v_t}e^{\left(\frac{v_{\rm mpp}+i_{\rm mpp}R_s}{v_t}\right)}}. \tag{16}$$

The parameters in (1) or (3) that best represent the output characteristics of the solar cell can be numerically determined by solving (14). Bisection, the Newton–Raphson method (NRM), and Secant [7] are examples of available numerical analysis methods. Although the parameterization previously described is only based on SSDM, it is easy to follow the same procedure and make $R_s = 0$ to determine the parameters in FSSDM.

E. Modeling Accuracy

To analyze the modeling accuracy of the proposed models, two popular types of PV modules made of polycrystalline silicon and CIS thin film are implemented and evaluated by the presented modeling methods. The specifications of the PV modules used in the evaluation are summarized in Table I.

Since the open-circuit voltage $V_{\rm oc}$ and short-circuit current $I_{\rm sc}$ are derived directly from the data obtained from experimental tests, there is no modeling error in SSDM and FSSDM at the points of open-circuit and short-circuit configurations. The matching accuracy at the MPPs and overall curve fitting performances need to be evaluated by comparing the model outputs with the experimentally measured data. To compare

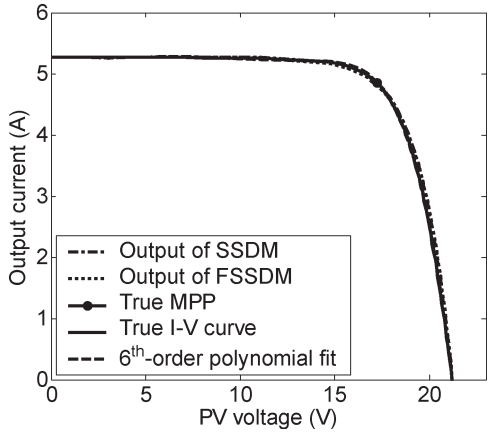

Fig. 5. $I-V$ curves of MSX-83 modeled by SSDM, FSSDM, and sixth-order polynomial.

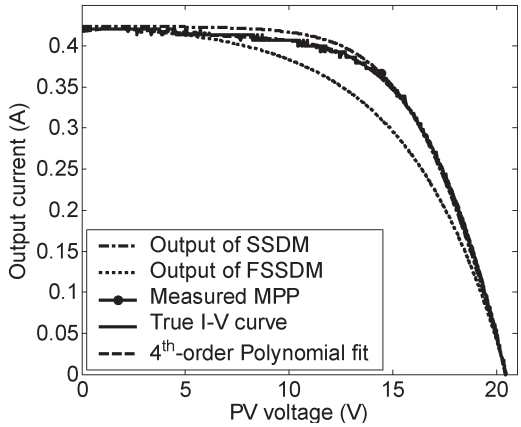

Fig. 6. $I-V$ curves of ST10 modeled by SSDM, FSSDM, and fourth-order polynomial.

different modeling methods correctly, the performance indexes are defined. The relative modeling error of the MPP is defined as

$$e_{\rm mpp} = \frac{|\hat{v}_{\rm mpp}\hat{i}_{\rm mpp} - v_{\rm mpp}i_{\rm mpp}|}{v_{\rm mpp}i_{\rm mpp}} \times 100 \tag{17}$$

where the point ($\hat{v}_{\rm mpp}$, $\hat{i}_{\rm mpp}$) is the estimated MPP derived by mathematical models and the point ($v_{\rm mpp}$, $i_{\rm mpp}$) represents the actual MPP.

The absolute voltage error of the optimal operating point is described as

$$e_{\rm OOP} = |\hat{v}_{\rm mpp} - v_{\rm mpp}| \tag{18}$$

where $\hat{v}_{\rm mpp}$ is the estimated voltage of the maximum operating point derived by mathematical models and $v_{\rm mpp}$ is the actual voltage of the maximum operating point.

The loss function used to demonstrate the curve fitting performance is defined as

$$\frac{\|\varepsilon\|_2}{\sqrt{m}} = \frac{\|\hat{I}_{\rm pv} - \tilde{I}_{\rm pv}\|_2}{\sqrt{m}} \tag{19}$$

where m is the number of samples, $\hat{I}_{\rm pv}$ is the vector of the estimated PV current, and $\tilde{I}_{\rm pv}$ is the vector of the measured PV current.

For the solar cells made of polycrystalline silicon, all the models of SSDM, FSSDM, and sixth-order polynomial show good-matching performance, as shown in Fig. 5. The $I-V$ curves of ST10 (CIS thin film) generated by the three different models are illustrated in Fig. 6. The data for modeling accuracy are summarized in Table II. The evaluations show that SSDM gives the most accurate estimation of MPP and the PCF models demonstrate the best curve fitting performance. The plots in Fig. 6 illustrate that FSSDM does not correctly represent the output features of the cells made of CIS thin film. The modeling error results from the simple structure and limited tuning parameters of FSSDM.

The accuracy of estimating the voltage of optimal operating point $V_{\rm OOP}$ is important since it represents the output of the MPP tracker and the reference for the voltage regulator in the presented MPPT scheme, as shown in Fig. 1. For the PV cells made of crystalline silicon, both the SSDM and FSSDM methods show good estimates of $V_{\rm OOP}$, as shown in Fig. 5. This is because both modeling processes are based on the MPP and contain the algorithm to minimize the modeling error at this point. The entries in Table II also show that the estimation of MPP in the PCF model is unfavorable because the least squares operation is designed to minimize the loss function of curve fitting and the matching of MPP is not considered into the modeling process. This situation can be improved by directly identifying the $P-V$ curve instead of the $I-V$ curve, as will be discussed in the following sections.

III. Real-Time Estimation of the MPP

Although SSDM shows good modeling performance for both types of PV cells according to Table II, the representation of the $I-V$ relationship makes the real-time application computation demanding due to the implicit form of (1). The solution to this equation with four unknowns requires a powerful digital signal processor. Based on the evaluation of the modeling accuracy in the last section, it was concluded that FSSDM is applicable for solar cells made of polycrystalline silicon, whereas the PCF is a general approach that describes the characteristics of PV cells made of either thin films or crystalline silicon. The advantage of the PCF is that it requires less demanding calculations compared with SSDM.

A. Parameter Estimation Based on FSSDM

In (3), thermal voltage v_t, saturation current $i_{\rm sat}$, and photocurrent $i_{\rm ph}$ are constant when there is no variation in insolation and cell temperature. These parameters of FSSDM can be determined with the measurements of PV voltage and output current. Then, the voltage of the optimal operating point $V_{\rm OOP}$ can be derived thereby. The detailed process of parameters is presented in [5]. This method requires four measurements of PV voltage and current.

TABLE II
COMPARISON OF THE MODELING ACCURACY OF SSDM, FSSDM, AND PCF

PV panels and Measured MPP	Models	$(\hat{v}_{mpp}, \hat{i}_{mpp})$	e_{mpp}	e_{mpop}	$\|\varepsilon\|_2$
MSX83	SSDM	(17.22V, 4.85A)	0.06%	0.007V	1.82×10^{-2}
Material: Crystalline silicon	FSSDM	(17.22V, 4.81A)	0.88%	0.007V	2.61×10^{-2}
Measured MPP:	PCF	(16.96V, 4.94A)	0.26%	0.270V	6.02×10^{-4}
(17.23V, 4.85A)					
Shell ST10	SSDM	(14.47V, 366mA)	0.07%	0V	5.89×10^{-5}
Material: CIS thin film	FSSDM	(14.47V, 312mA)	14.70%	0V	9.35×10^{-4}
Measured MPP:	PCF	(14.65V, 356mA)	1.45%	0.18V	6.59×10^{-6}
(14.46V, 366mA)					

B. Recursive Parameterization of Polynomial Models

In a solar power system, parameters change continuously with variation of insolation and cell temperature, and parameter observations are obtained sequentially in real time. Therefore, it is desirable to make the computation recursively to save computation time. By using the recursive least squares estimation (RLS) [6], the parameters of the system model are obtained by minimizing the error between prediction and measurement. The vector of the estimated parameters $\hat{\theta}$ is updated as

$$\hat{\theta}(k) = \hat{\theta}(k-1) + M(k)\left[y(k) - \hat{y}(k)\right] \tag{20}$$

where $\hat{\theta}(k-1)$ is the previous estimation, the components of vector $M(k)$ are the weighting factors that determine the correction, $y(k)$ is the measurement, and $\hat{y}(k)$ is the prediction based on the previous parameter estimate. The predictions and corrections are operated recursively in real time to make the model estimation accurate. The RLS estimate can also be interpreted as a Kalman filter [6]. In MPPT, the $P-V$ curve of the PV array is more useful than the $I-V$ curve since the former clearly shows the situation of MPP. Therefore, the proposed modeling process is based on the relationship of the power and voltage outputted by the PV panels. Considering a panel made of thin film, the output power is represented by

$$p(k) = b_1(k)v(k) + b_2(k)v^2(k) + b_3(k)v^3(k) + b_4(k)v^4(k) \tag{21}$$

where b_i are the model parameters that change with environmental conditions and $v(k)$ is the voltage output. For convenience, they are defined as

$$\theta(k) = \begin{bmatrix} b_1(k) \\ b_2(k) \\ b_3(k) \\ b_4(k) \end{bmatrix} \quad \varphi(k) = \begin{bmatrix} v(k) \\ v^2(k) \\ v^3(k) \\ v^4(k) \end{bmatrix}. \tag{22}$$

Therefore, (21) can be written as

$$p(k) = \varphi^T(k)\theta(k). \tag{23}$$

According to the theorem of RLS in [6], the estimation of parameter vector $\hat{\theta}$ can be obtained by satisfying the following recursive equations:

$$\hat{\theta}(k) = \hat{\theta}(k-1) + M(k)\left[p(k) - \varphi^T(k)\hat{\theta}(k-1)\right] \tag{24}$$

$$M(k) = W(k)\varphi(k) = \frac{W(k-1)\varphi(k)}{\lambda + \varphi^T(k)W(k-1)\varphi(k)} \tag{25}$$

$$W(k) = \frac{\left[I - M(k)\varphi^T(k)\right]W(k-1)}{\lambda} \tag{26}$$

where $p(k)$ represents the measured power condition, $M(k)$ is the weighting factor that determines the direction of correction, $W(k)$ is a nonsingular matrix defined for the RLS operation, and λ is the forgetting factor that ranges from zero to unity. The parameters of the proposed model are time varying due to variation of insolation and temperature, so the forgetting factor is needed to base the identification on recent data rather than old data. The recursive equations need to start with the initial conditions, which are matrix $W(0)$ and vector $\hat{\theta}(0)$. The identification process is illustrated by a flowchart, as shown in Fig. 7.

C. Determination of the Voltage of the Optimal Operating Point

As analyzed in Section II, $V_{\rm OOP}$ satisfies the condition

$$\left.\frac{dp}{dv}\right|_{v=V_{\rm OOP}} = 0 \tag{27}$$

where p is the output power and v is the PV voltage. For convenience, it is defined by

$$f(v) = \frac{dp}{dv}. \tag{28}$$

Then, $V_{\rm OOP}$ can be found by setting $f(v) = 0$. This can be solved by using the NRM [7]. This numerical solution requires the derivative $f'(v)$ to be computed.

In FSSDM (2),

$$f(v) = \frac{dp}{dv} = i_{\rm ph} + i_{\rm sat}\left[1 - \left(\frac{v}{v_t} + 1\right)e^{\left(\frac{v}{v_t}\right)}\right] \tag{29}$$

$$f'(v) = \frac{d^2p}{dv^2} = -i_{\rm sat}e^{\left(\frac{v}{v_t}\right)}\frac{1}{v_t}\left(\frac{v}{v_t} + 2\right). \tag{30}$$

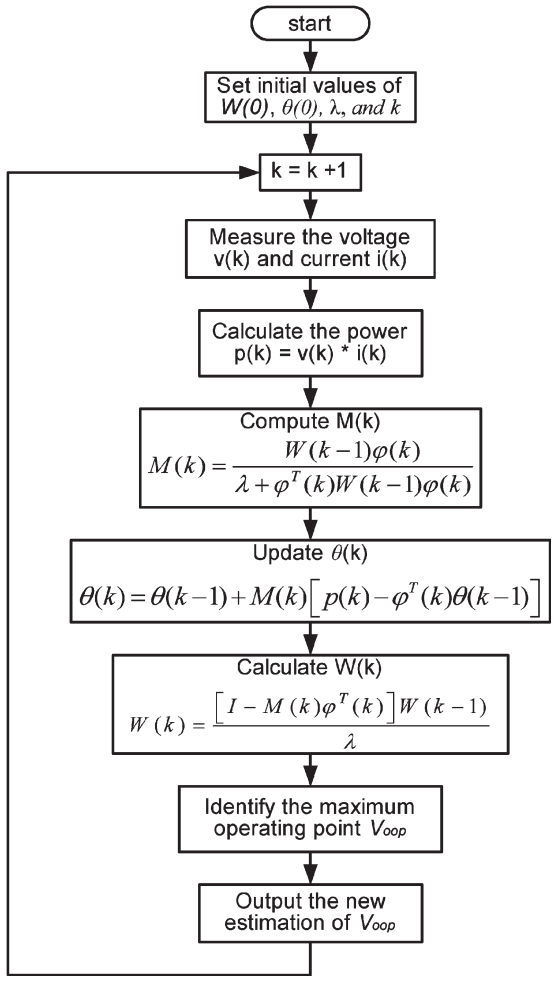

Fig. 7. Flowchart of the RLS estimation procedure to determine the system parameters.

With the correctly identified parameters of the fourth-order PCF model (21), $V_{\rm OOP}$ can be found to make

$$f(v)=\frac{dp}{dv}=\hat{b}_1+2\hat{b}_2v+3\hat{b}_3v^2+4\hat{b}_4v^3=0 \tag{31}$$

where the parameters $\hat{b}_i$ are estimated. In the mathematical model, $f'(v)$ can be calculated as

$$f'(v)=\frac{d^2p}{dv^2}=2\hat{b}_2+6\hat{b}_3v+12\hat{b}_4v^2. \tag{32}$$

The flowchart that illustrates NRM's iteration operation in finding the roots of $f(v)=0$ is demonstrated in Fig. 8.

D. Convergence Analysis

Convergence is the most fundamental design requirement of system identification and numerical solvers. The exponential forgetting of data was the technique chosen to identify the time-varying parameters of PV panels changing with insolation and temperature. When a constant forgetting factor is used in the application of RLS, the smaller the forgetting factor λ, the faster the algorithm can track the parameters. However, a small λ may lead to an unstable estimation by causing matrix

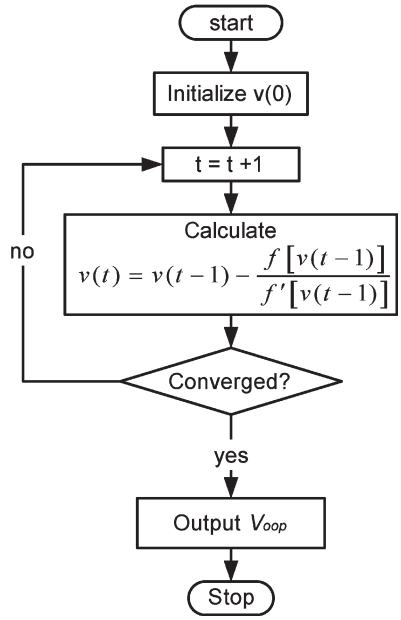

Fig. 8. Flowchart of the NRM operation in finding $V_{\rm OOP}$.

W to blow up [8]. It is desirable to make the λ adaptive to the change of system dynamics. Many effective solutions to this problem in real-time system identification are found in [8]–[11]. In this paper, the forgetting factor is adjusted according to the prediction error as

$$\lambda(n)=1-k\varepsilon^2(n), \qquad 0\le k\le\frac{1}{10\varepsilon^2_{\max}} \tag{33}$$

$$\varepsilon(n)=y(n)-\hat{y}(n) \tag{34}$$

where k is a parameter chosen according to system dynamics, ε represents the error between the prediction and measurement of the output power $y(n)$, and $\varepsilon_{\max}$ is the maximum error. In MPPT system, the dominant factor shifting the $V_{\rm OOP}$ is the cell temperature. Generally, the cell temperature in PV power systems shows slow dynamics since a sudden increase or decrease of temperature seldom occurs. Therefore, the forgetting factor needs to be tuned properly according to the dynamics caused by the change in temperature.

The NRM is a fast approach in finding the roots of $f(v)$, but it does not always converge. It is known that the choice of the initial value $v(0)$ is critical to avoid the divergence from the root and to prevent the problem of division by zero when

$$\frac{df}{dv}=0. \tag{35}$$

To demonstrate this problem, the relationship of $f(v)$ and v is illustrated in Fig. 9. Point A represents the short-circuit situation, point B is the point that causes division by zero, point C is the MPP need to be identified, and point D symbolizes the open-circuit condition. Through the analysis of this plot, the convergence is guaranteed if the initial value of PV voltage is chosen in the interval (E, D). Generally, it is recommended to choose the initial value for NRM ranging from the possible $V_{\rm OOP}$, which is point F, to the open-circuit voltage, which is point D, to avoid this divergence problem.

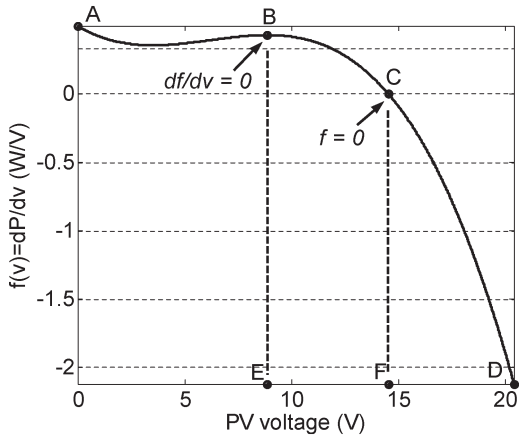

Fig. 9. Relationship of $f(v)$ and v.

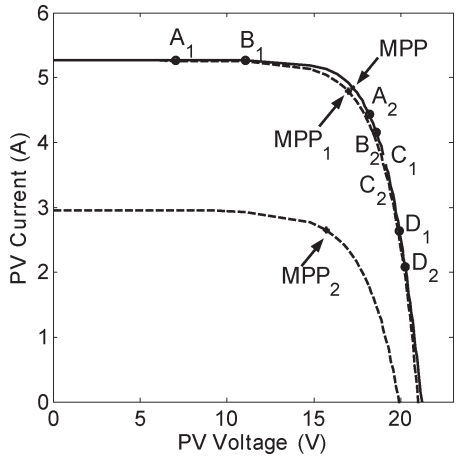

Fig. 10. Estimated $I-V$ curves and MPPs with FSSDM.

IV. Evaluations

It is realized that the distribution of the selected points used in FSSDM is sensitive to the estimation accuracy. This problem is demonstrated by the FSSDM estimation process of an MSX-83 solar module made of crystalline silicon. The experimental $I-V$ curve is shown in Fig. 10 in a solid line, and the estimated $I-V$ curves are illustrated by dashed lines.

When the four points A_1, B_1, C_1, and D_1 are chosen, the prediction gives a reasonable result MPP_1, and indicates that $V_{\mathrm{OOP}} = 16.95$ V compared to the actual V_{OOP} of 17.22V. When another four points A_2, B_2, C_2, and D_2 are selected in the evaluation, the estimation shows an incorrect MPP, MPP_2, illustrating $V_{\mathrm{OOP}} = 15.71$ V, which is far from the true value. The numerical differentiation in [5] based on the four points may cause estimation inaccuracy for certain distributions of points. For example, this occurs when the points are sampled such that the respective slope of each point is similar to that of the others. In PV power systems, the MPPT controller regulates the operating point around the MPP for maximum solar power. These issues make it difficult to use FSSDM in the real-time estimation since the accuracy of the estimation cannot be guaranteed. The advantage of the polynomial model is that

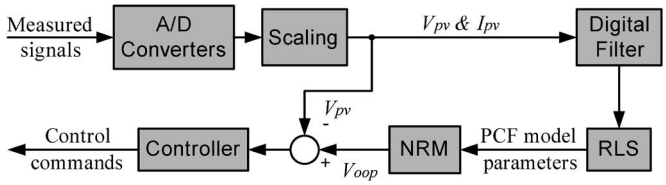

Fig. 11. Control structure of MPPT with real-time identification.

the method of RLS continuously minimizes the modeling error during the real-time operation. Furthermore, the existing techniques of RLS assure that the estimated parameters converge to the true values. Therefore, the evaluation results described in the following paragraphs are based on the real-time estimation of the polynomial model, as discussed in Section III.

The effectiveness of the proposal with PCF is verified by both computer simulation and experimental tests. During the system operation, the controller senses both the voltage and current of a PV array, while the identification process runs simultaneously to reveal the estimated V_{OOP}, as shown in Fig. 11. The value of V_{OOP} is identified by RLS and NRM. It is used as the reference in the regulation loop of the PV voltage. The low-pass digital filter facilitates the attenuation of the high-frequency noise, which may otherwise lead to incorrect estimates. A finite-impulse response (FIR) filter is applied in the proposed system to improve its stability. For an N-tap FIR filter, the output is described by

$$y(k) = \sum_{n=0}^{N-1} \left[h(n)x(k-n) \right]. \tag{36}$$

The FIR filter is specified by the filter coefficient $h(n)$ and the output sequence $y(k)$ for the input sequence $x(k)$ by discrete convolution. The major problem with the FIR filter design is the definition of $h(n)$. However, this can be solved using a software tool such as Matlab.

A. Simulation

It is known that temperature is the dominant factor that affects the value of V_{OOP}. The variation of cell temperature primarily depends on the insolation level, ambient temperature, and cell conduction loss. The simulation is designed to show the effect of the constant irradiance on cell surface and the continuous conduction through the PV cells will cause a gradual increase in cell temperature. As shown in Fig. 12, these phenomena will reduce the PV output power and shift the voltage of optimal operating point to lower levels until thermal balance is reached.

During system operation, the PV voltage is supposed to be regulated at a constant level, which is a typical operation mode in PV power systems. The performance is evaluated by comparing the estimated V_{OOP} to the true V_{OOP} measured in real time. It is clearly noticed in Fig. 12 that the value of the estimated V_{OOP} smoothly decreases, following the change of the actual V_{OOP} caused by the continuous increasing of cell temperature, and converges with the actual V_{OOP} when thermal balance is reached. The plot also shows the unavoidable time

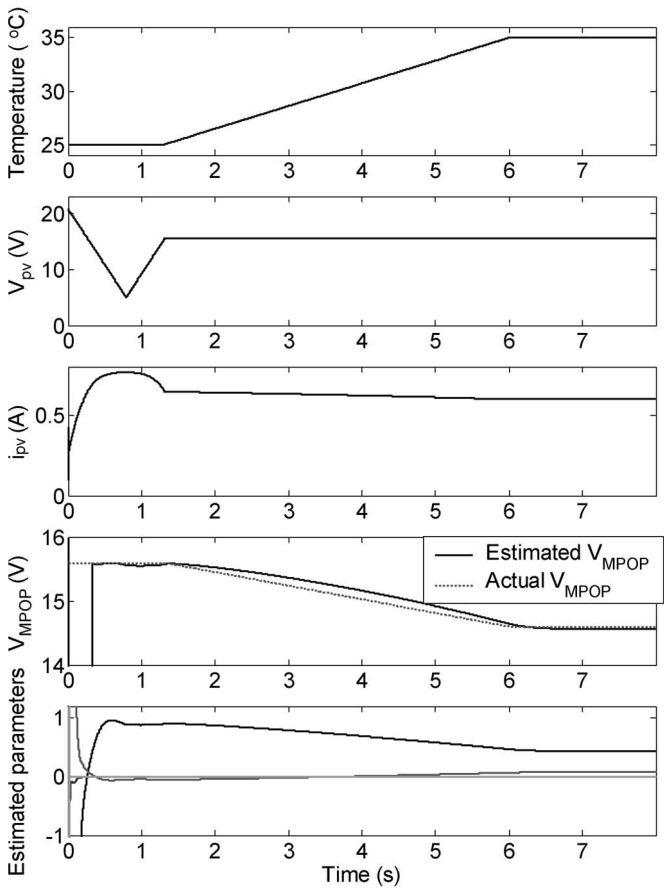

Fig. 12. Simulated plots of the changes of temperature, PV voltage, PV current, $V_{\rm OOP}$, and estimated parameters when the temperature increases from 25 °C to 35 °C with a constant insolation of 1000 W/m^2.

delay in estimation during the real-time operation. The plots also show the variation of parameters, which is caused by the temperature change and estimated by the RLS operation in real time.

B. Experimental Evaluation

The validity of the proposed identification method was examined with a PV panel and natural solar irradiance. As illustrated in Fig. 13, the operating point of the PV panel can be varied randomly by adjusting the load condition. The transducers sense the voltage and current of the panel output, and the data acquisition system (DAQ) provides the interface between the transducers and the personal computer (PC). With the measurements, real-time identification is performed by using a computer software (Matlab). The value of k in (33) is set to 0.005. The testing specification is listed in Table III.

In the beginning, the PCF of the $P-V$ characteristics and the identification of $V_{\rm OOP}$ are analyzed offline with the measured voltage and current of the PV outputs. The experimental results show that the $P-V$ curve is successfully recovered by the RLS operation, and $V_{\rm OOP}$ is estimated accurately by NRM, as shown in Fig. 14.

Furthermore, the operating points of the PV panel are adjusted in a large range by varying the load conditions. The PV voltage and current are measured in real time, as illustrated in

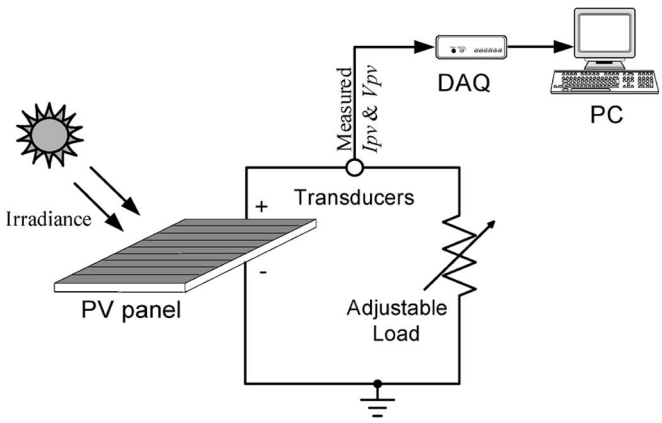

Fig. 13. Block diagram of the experimental evaluation.

TABLE III
EXPERIMENTAL TEST ENVIRONMENT

Photovoltaic module:	Shell ST10 (CIS/thin film)
Testing conditions:	Sunny day, no cloud Ambient temperature: 25.3°C
Load condition:	Resistive load: Resistance ranges from 0Ω to infinity
Data acquisition system:	Labview™ DAQ board and software

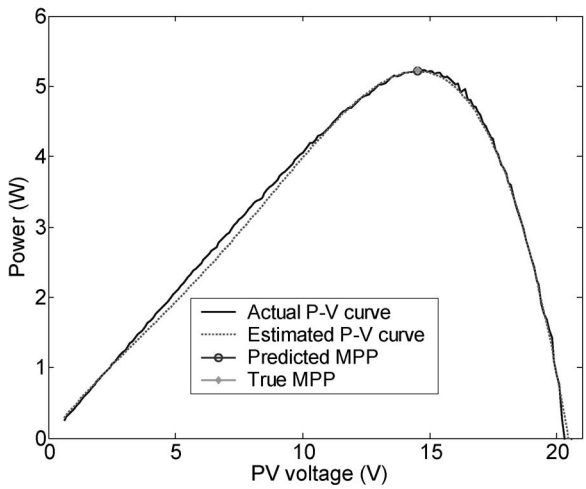

Fig. 14. Plots of offline curve fitting and estimation of $V_{\rm OOP}$ by RLS and NRM.

Fig. 15(a) and (b), and are used to estimate the system parameters and to identify $V_{\rm OOP}$ in real time. During the test period, the measured MPP is constant at point (14.51 V, 0.366 A). The plot shows that the model parameters are successfully identified after the initial condition. The $V_{\rm OOP}$ converges to a steady value of 14.53 V and does not change with the variations of operating points, as illustrated in Fig. 15(c). The experimental results show some minor variations in the model parameters, which are illustrated in Fig. 15(d). These have insignificant impact on the estimation of $V_{\rm OOP}$. The estimation error in steady state is less than 0.14%, which is more accurate than the identification based on the $I-V$ curve demonstrated in Section II.

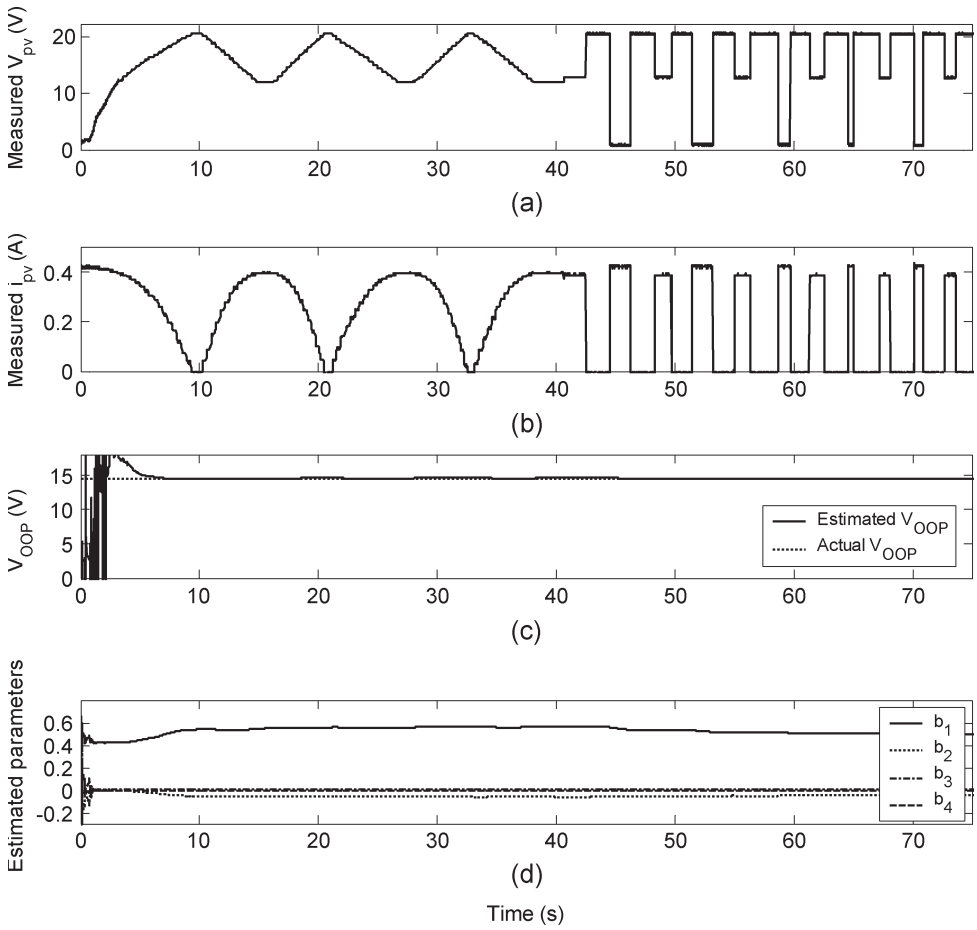

Fig. 15. Estimation process of V_{OOP} and parameters using RLS and NRM.

TABLE IV
MODELING FEATURES OF EQUIVALENT CIRCUIT AND POLYNOMIAL CURVE FITTING

Models	Equivalent circuit	Polynomial curve fitting
Pros	□ It has physical meaning. □ It demonstrates the features of cell output in terms of environment changes in irradiance and temperature. □ It requires only three or four points for modeling process. □ It demonstrates good performance in offline modeling.	□ It is an ideal mathematical model useful for parameter identifications and numerical solutions in real time. □ The overall modeling error is minimized when the least-square method is used.
Cons	□ It is difficult to be solved by analytical methods.	□ It is a pure mathematical representation, no physical link with the material. □ The modeling accuracy is related to the number of available measurements.

V. CONCLUSION

A general real-time identification method has been proposed to estimate the optimal operating point in PV power systems in an adaptive fashion. It uses polynomials to demonstrate the electric characteristics of PV panels. This makes the application of the RLS and NRM method computations less demanding since they effectively identify the voltage variation of the optimal operating point V_{OOP}. This point is the key parameter in the operation of MPPT. Such variation in V_{OOP} could be caused by the change of insolation, temperature, and aging. The effectiveness of the proposed methods is demonstrated by computer simulations and experimental evaluation. The experimental test shows that the estimation error of V_{OOP} in steady state is less than 0.14%. It is also discovered that the polynomial model based on the power–voltage relationship, which is the $P-V$ curve, of PV panels shows more accurate estimation on V_{OOP} than using the model of the $I-V$ curve.

In this paper, the major modeling features of the equivalent circuit and PCF are analyzed and summarized in Table IV. Although FSSDM is applicable in real-time prediction for cells

made of silicon, the estimation accuracy is sensitive to the distribution of the selected measurement points. This makes the identification unavailable to use FSSDM in real time because the system only operates the voltage of the PV array in a certain range, which may not cover the range of measurements required by the modeling process.

Despite the focus of the evaluation on the PV module made of CIS thin film, the same concept can be applied to the panels made of polycrystalline silicon when the sixth-order polynomial models are adopted. It is proved that the polynomial equation is a general approach in modeling PV modules made of crystalline silicon and CIS thin film.

ACKNOWLEDGMENT

The authors would like to thank Dr. D. Birnie from Rutgers, The State University of New Jersey, for providing the experimental $I-V$ data of the SolarEx MSX-83 module as a function of temperature at his website. The SolarEx MSX-83 module is a product of BP Solar.

REFERENCES

[1] C. Hua, J. Lin, and C. Shen, "Implementation of a DSP-controlled photovoltaic system with peak power tracking," *IEEE Trans. Ind. Electron.*, vol. 45, no. 1, pp. 99–107, Feb. 1998.

[2] K. H. Hussein, I. Muta, T. Hoshino, and M. Osakada, "Maximum photovoltaic power tracking: An algorithm for rapidly changing atmospheric conditions," in *Proc. IEE Generation, Transmiss., Distrib.*, Jan. 1995, vol. 142, pp. 59–64.

[3] S. Liu and R. A. Dougal, "Dynamic multiphysics model for solar array," *IEEE Trans. Energy Convers.*, vol. 17, no. 2, pp. 285–294, Jun. 2002.

[4] W. Xiao and W. G. Dunford, "A novel modeling method for photovoltaic cells," in *Proc. IEEE PESC*, 2004, pp. 1177–1183.

[5] A. Capel, L. M. Salamero, W. Xiao, and W. G. Dunford, "A novel approach to operate solar arrays at their MPP without tracking process," in *Proc. Annu. Seminar Autom. Control, Ind. Electron. and Instrum.*, 2004, pp. 229–232.

[6] K. J. Astrom and B. Wittenmark, *Adaptive Control*. Reading, MA: Addison-Wesley, 1995, pp. 41–89.

[7] G. Recktenwald, *Numerical Methods With MATLAB: Implementations and Applications*. Englewood Cliffs, NJ: Prentice-Hall, 2000, pp. 240–273.

[8] S. H. An and K. Yao, "Convergent and roundoff error properties of reflection coefficients in adaptive spatial recursive least squares lattice algorithm," *IEEE Trans. Circuits Syst.*, vol. 35, no. 2, pp. 241–246, Feb. 1988.

[9] M. E. Salgado, G. C. Goodwin, and R. H. Middleleton, "Modified least square algorithm incorporating exponential resetting and forgetting," *Int. J. Control*, vol. 47, no. 2, pp. 477–491, Jan. 1988.

[10] T. R. Fortesque, L. S. Kershenbaum, and B. E. Ydstie, "Implementation of self tuning regulators with variable forgetting factors," *Automatica*, vol. 17, no. 6, pp. 831–835, Nov. 1981.

[11] J. Slotine and W. Li, *Applied Nonlinear Control*. Englewood Cliffs, NJ: Prentice-Hall, 1991, pp. 376–382.

Weidong Xiao (S'03) received the M.A.Sc. degree in electrical engineering in 2003 from the University of British Columbia, Vancouver, BC, Canada, where he is currently working toward the Ph.D. degree at the University of British Columbia.

His research interests include power electronics and applications of renewable energy sources.

Magnus G. J. Lind (S'04) received the B.S.E.E.T. degree from Western Washington University, Bellingham, in 2002, and the Ph.D. degree from the University of British Columbia, Vancouver, BC, Canada, in 2006.

He is an Electrical Engineer with the PACCAR Technical Center Inc., Mount Vernon, WA.

William G. Dunford (M'81–SM'92) received the degree in engineering from Imperial College, London, U.K., and the Ph.D. degree from the University of Toronto, Toronto, ON, Canada.

He was a Faculty Member with Imperial College and the University of Toronto and held positions in the Royal Aircraft Establishment, Schlumberger, and Alcatel. He is currently an Associate Professor at the University of British Columbia, Vancouver, BC, Canada. His research interests include photovoltaic power systems, automotive, energy harvesting, and biological monitoring.

Dr. Dunford has served in various positions in the Advisory Committee of the IEEE Power Electronics Society and was the Chair of the IEEE Power Electronics Specialists Conference in 1986 and 2001.

Antoine Capel received the Ph.D. degree from the University of Toulouse, Toulouse, France.

After teaching at Toulouse and at the University of Pernambouc, Brazil, he joined the European Space Agency as a Power System Engineer. In 1983, he joined Alcatel Espace, Toulouse, France, where he first managed the Power Supply Laboratory and was the Head of the Power System Simulation Division until his retirement. He is currently an Adjunct Professor at the University of British Columbia, Vancouver, BC, Canada, and the Universitat Rovira i Virgili, Spain.

Dr. Capel served as the General Chair of IEEE PESC'85 in Toulouse.